





Physics-Informed Neural Networks for Tissue Elasticity Reconstruction in Magnetic Resonance Elastography

Matthew Ragoza¹(✉)  and Kayhan Batmanghelich² 

¹ University of Pittsburgh, Pittsburgh, PA 15213, USA
mtr22@pitt.edu

² Boston University, Boston, MA 02215, USA

Abstract. Magnetic resonance elastography (MRE) is a medical imaging modality that non-invasively quantifies tissue stiffness (elasticity) and is commonly used for diagnosing liver fibrosis. Constructing an elasticity map of tissue requires solving an inverse problem involving a partial differential equation (PDE). Current numerical techniques to solve the inverse problem are noise-sensitive and require explicit specification of physical relationships. In this work, we apply physics-informed neural networks to solve the inverse problem of tissue elasticity reconstruction. Our method does not rely on numerical differentiation and can be extended to learn relevant correlations from anatomical images while respecting physical constraints. We evaluate our approach on simulated data and *in vivo* data from a cohort of patients with non-alcoholic fatty liver disease (NAFLD). Compared to numerical baselines, our method is more robust to noise and more accurate on realistic data, and its performance is further enhanced by incorporating anatomical information.

Keywords: Physics-informed learning · Magnetic resonance elastography · Elasticity reconstruction · Deep learning · Medical imaging

1 Introduction

Tissue elasticity holds enormous diagnostic value for detecting pathological conditions such as liver fibrosis [1, 2] and can be mapped by an imaging procedure called magnetic resonance elastography (MRE). During MRE, a mechanical stress is applied to the region of interest and an image is captured of the resulting tissue deformation, then the elasticity is inferred by solving the inverse problem of a partial differential equation (PDE). However, conventional methods for elasticity reconstruction are sensitive to noise, do not incorporate anatomical information, and are often only evaluated on artificial data sets [3–8].

Supplementary Information The online version contains supplementary material available at https://doi.org/10.1007/978-3-031-43999-5_32.

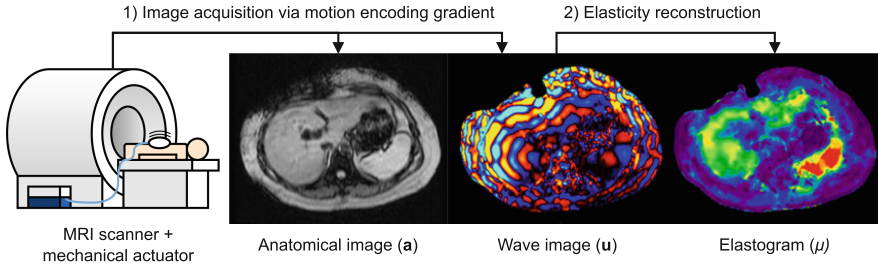


Fig. 1. During MRE, a mechanical actuator induces shear waves while a motion-encoding gradient captures the tissue deformation as a wave image. Then, an inverse problem is solved to reconstruct a map of tissue elasticity called an elastogram.

Elasticity reconstruction methods utilize a variety of numerical techniques and physical models [9]. Algebraic Helmholtz inversion (AHI) makes simplifying assumptions that enable an algebraic solution to the governing equations [3, 5]. However, AHI relies on finite differences, which amplify noise. The finite element method (FEM) requires fewer physical assumptions and solves a variational formulation of the PDE [4, 6–8, 10], making it more flexible and typically more robust than AHI. However, neither method uses anatomical images, which have been successfully used to predict elasticity with deep learning [11–13].

Physics-informed neural networks (PINNs) are a recent deep learning framework that uses neural networks to solve PDEs [14]. PINNs represent unknown function(s) in a boundary value problem as neural networks. The boundary conditions and PDE are treated as loss functions and the problem is solved using gradient-based optimization. PINNs have been applied to elasticity reconstruction in other contexts [15–18], but evaluations have been limited to artificial data sets and prior work has not combined physics-informed learning with automated learning from anatomical MRI.

In this work, we develop a method for enhanced tissue elasticity reconstruction in MR elastography using physics-informed learning. We use PINNs to solve the equations of linear elasticity as an optimization problem for a given wave image. Our model simultaneously learns continuous representations of the measured displacement field and the latent elasticity field. We evaluate the method on a numerical simulation and on patient liver MRE data, where we demonstrate improved noise robustness and overall accuracy than AHI or FEM-based inversion. In addition, we show that augmenting our method with an anatomically-informed loss function further improves reconstruction quality.

2 Background

Magnetic Resonance Elastography (MRE). An MRE procedure involves placing the patient in an MRI scanner and using a mechanical actuator to induce shear waves in the region of interest (Fig. 1). A motion-encoding gradient (MEG) synchronizes with the mechanical vibration, causing phase shifts in the captured

Table 1. Physical equations relating the displacement field \mathbf{u} to the shear modulus of elasticity μ during a steady-state harmonic motion from the theory of linear elasticity.

Name	Assumptions		Equation
	$\nabla \cdot \mathbf{u} = 0$	$\nabla \mu = 0$	$\mathcal{D}(\mu, \mathbf{u}, \mathbf{x}) = 0$
general form			$\nabla \cdot [\mu (\nabla \mathbf{u} + \nabla \mathbf{u}^\top) + \lambda (\nabla \cdot \mathbf{u}) \mathbf{I}] + \rho \omega^2 \mathbf{u} = 0$
heterogeneous	✓		$\mu \nabla^2 \mathbf{u} + (\nabla \mathbf{u} + \nabla \mathbf{u}^\top) \nabla \mu + \rho \omega^2 \mathbf{u} = 0$
Helmholtz	✓	✓	$\mu \nabla^2 \mathbf{u} + \rho \omega^2 \mathbf{u} = 0$

signal based on the tissue displacement [19]. A *wave image* that encodes the full 3D displacement field can be acquired using MEGs in each dimension [1]. Next, a map of tissue stiffness called an *elastogram* is recovered from the wave image by solving an inverse problem. This requires 1) choosing a physical model that relates the motion of an elastic body to its material properties, and 2) solving the governing equation(s) for the unknown material parameters.

Linear Elasticity. Physical models of MRE typically assume there is harmonic motion and a linear, isotropic stress-strain relation. Then tissue displacement is a complex vector field $\mathbf{u} : \Omega \rightarrow \mathbb{C}^3$ defined on spatial domain $\Omega \subset \mathbb{R}^3$, and shear elasticity is characterized by the *shear modulus*, a complex scalar field $\mu : \Omega \rightarrow \mathbb{C}$. The first equation of motion translates into the *general form* PDE shown in Table 1. The mass density ρ and actuator frequency ω are prescribed based on prior knowledge. The Lamé parameter λ can be ignored if we assume tissue is incompressible ($\nabla \cdot \mathbf{u} = 0$), reducing the PDE to the *heterogeneous form*. Finally, assuming that the shear modulus is locally homogeneous ($\nabla \mu = 0$) simplifies the PDE into the *Helmholtz equation*. The empirical validity of the homogeneity assumption has been criticized [20, 21] and is explored in our experiments.

3 Proposed Method

We use physics-informed neural networks (PINNs) to encode the solution space of the inverse problem. Our PINN framework (Fig. 2) learns continuous representations of the displacement field $\mathbf{u}(\mathbf{x})$ and elastic modulus $\mu(\mathbf{x})$ while respecting a PDE from Table 1. We incorporate conventional MRI images by including an additional anatomically-informed loss function. In the following sections, we explain the PINN framework and how we incorporate the anatomical images.

Physics-Informed Neural Networks. We use a dual-network approach to reconstruct tissue elasticity with PINNs. First, we train a neural network $\hat{\mathbf{u}}(\mathbf{x}; \theta^u)$ to learn a mapping from spatial coordinates \mathbf{x} to displacement vectors \mathbf{u} in the wave image by minimizing the mean squared error \mathcal{L}_{wave} . The continuous representation of the displacement field enables automatic spatial differentiation.

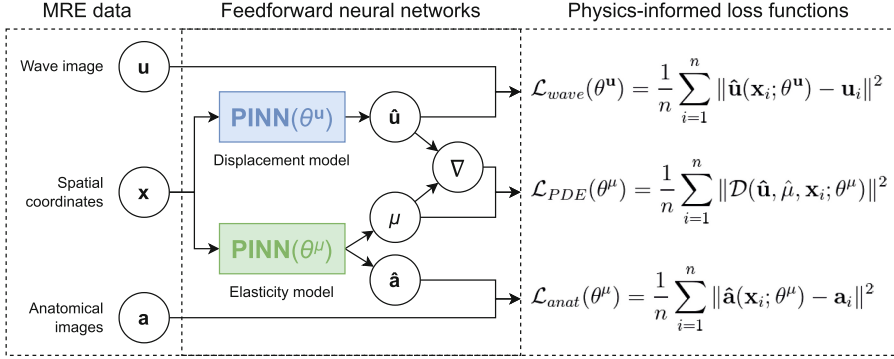


Fig. 2. In our framework, one PINN learns to map from spatial coordinates to displacement vectors by fitting to the wave image, while another learns to recover the shear elasticity at the corresponding position by minimizing a PDE residual. The elasticity model can also predict anatomical MRI features that are correlated with elasticity. Note that the PINNs are trained to fit a set of images for a single patient/phantom and that n represents the number of (spatial coordinate, image value) pairs per batch.

Then, we train a second neural network $\hat{\mu}(\mathbf{x}; \theta^{\mu})$ to map from spatial coordinates to the shear modulus μ by minimizing the residual of a PDE, defined by some differential operator \mathcal{D} . The PINNs and their spatial derivatives are used to evaluate the differential operator, which is minimized as a loss function \mathcal{L}_{PDE} to recover the elasticity field. We combine the loss functions as follows:

$$\mathcal{L}(\theta^{\mathbf{u}}, \theta^{\mu}) = \lambda_{\text{wave}} \mathcal{L}_{\text{wave}}(\theta^{\mathbf{u}}) + \lambda_{\text{PDE}} \mathcal{L}_{\text{PDE}}(\theta^{\mu})$$

We train PINNs using either the Helmholtz equation (PINN-HH) or the heterogeneous PDE (PINN-het) as the differential operator \mathcal{D} in our experiments. The loss weight hyperparameters λ_{wave} and λ_{PDE} control the contribution of each loss function to the overall objective. We initialized λ_{PDE} to a very low value and slowly stepped it up as the quality of $\hat{\mathbf{u}}$ improved during training.

Incorporating Anatomical Information. Prior work has demonstrated that tissue elasticity can be accurately predicted from anatomical MRI [22]. We include an additional output head $\hat{\mathbf{a}}(\mathbf{x}; \theta^{\mu})$ from the elasticity PINN that predicts anatomical features $\mathbf{a}(\mathbf{x})$ at the corresponding position, as encoded in standard MRI imaging sequences. Then we introduce an additional loss function $\mathcal{L}_{\text{anat}}$ to minimize the mean squared error between the predicted and true anatomical features. We explore how the relative weight of this loss function λ_{anat} affects elasticity reconstruction performance in our *in vivo* experiments.

We designed our models based on the SIREN architecture, which uses sine activation functions to better represent high spatial frequencies [23]. Both networks $\hat{\mathbf{u}}$ and $\hat{\mu}$ had five linear layers with 128 hidden units per layer and dense connections from all previous layer inputs. The first layer input was scaled by

a hyperparameter ω_0 that biases the initial spatial frequency distribution. We employed the weight initialization scheme described in [23] to improve training convergence. We also extended the input vector with polar coordinates when training on patient data. We trained all models for 100,000 total iterations with the Adam optimizer using PyTorch v1.12.1 and DeepXDE v1.5.1 [24–26]. The code used for this work is available at <https://github.com/batmanlab/MRE-PINN>.

4 Related Work

Algebraic Helmholtz Inversion (AHI). One of the most common methods for elasticity reconstruction is algebraic inversion of the Helmholtz equation (AHI) [3]. This approach assumes incompressibility and local homogeneity, uses finite differences to compute the Laplacian of the wave image, and then solves the Helmholtz equation as a linear system to estimate the shear modulus. Despite its simplicity, AHI has an established track record in both research and clinical settings [9]. Filtering is often required to reduce the impact of noise on AHI [5].

Finite Element Method (FEM). Many techniques have been introduced for elasticity reconstruction based on the finite element method [4, 6, 7, 10]. These use variational formulations to reduce the order of differentiation in the PDE. Then, they specify a mesh over the domain and represent unknown fields in terms of compact basis functions. This results in a linear system that can be solved for the elasticity coefficients either directly or iteratively [9]. Direct FEM inversion is more efficient and accurate [21], though it depends more on data quality [8]. We implemented direct FEM inversion of the Helmholtz equation (FEM-HH) and the heterogeneous PDE (FEM-het) with FEniCSx v0.5.1 [27].

5 Experiments and Results

We compare our methods (PINN-HH, PINN-het) to algebraic Helmholtz inversion (AHI) and direct FEM inversion (FEM-HH, FEM-het) on simulated data and liver data from a cohort of patients with NAFLD. We evaluate the overall reconstruction fidelity of each method and the impact of the homogeneity assumption. We assess their robustness to noise on the simulated data, and we study whether incorporating anatomical images enhances performance on patient liver data.

5.1 Robustness to Noise on Simulated Data

We obtained a numerical FEM simulation of an elastic wave in an incompressible rectangular domain containing four stiff targets of decreasing size from the BIOQIC research group (described in Barnhill et. al. 2018 [28]). Six wave fields were generated at frequencies ranging from 50–100 Hz in 10 Hz increments. We applied each reconstruction method to each single-frequency wave image after adding varying levels of Gaussian noise. Then we computed the contrast transfer efficiency (CTE) [29] in each target region as the ratio between the target-background contrast in the predicted elastogram and the true contrast, where a CTE of 100% is ideal. We include functions to download the simulation data set in the project codebase.

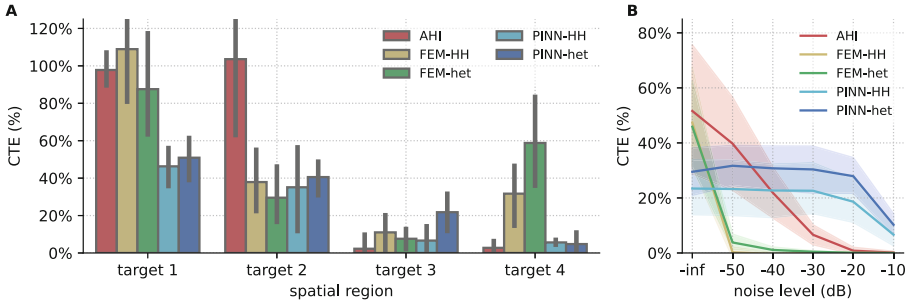


Fig. 3. Reconstruction performance on simulated data. Figure 3A shows the contrast transfer efficiency of each method in each target region of the simulation. Figure 3B shows how the contrast is affected by the noise level in the wave image.

Experiment Results. Figure 3A compares the CTE of each method in the different target regions of the simulation, which decrease in size from left to right. On target 1, AHI performs best with 98% CTE followed by FEM-HH and FEM-het with 109% and 88%. PINN-HH and PINN-het had 46% and 51% contrast on target 1. AHI also performed best on target 2, with 104% CTE. Next were PINN-het with 41% contrast and FEM-HH with 38%. PINN-het outperformed the other methods on target 3 with 22% CTE followed by FEM-HH with 11%. Only the two FEM methods appear to have decent contrast on target 4, though this seems to be a false positive due to background variance seen in Fig. 4.

Figure 3B shows the effect of wave image noise on the contrast transfer efficiency. The reconstruction quality decays at -50 db of noise for both FEM-HH ($p = -1.7e-5$) and FEM-het ($p = 9.1e-6$), each retaining less than 5% contrast. AHI is also sensitive to -50 dB of noise ($p = 6.1e-4$) but its performance drops more gradually. The contrast from PINN-HH does not decrease significantly until -20 dB ($p = 8.8e-4$) and PINN-het is insensitive until -10 dB ($p = 4.8e-5$). This indicates that PINNs are more robust to noise than AHI or direct FEM.

Figure 4 displays reconstructed elastograms from each method using the 90Hz simulated wave image, displayed at far left, next to the ground truth. AHI produces the clearest boundaries between the targets and background. The two FEM methods contain high variability within homogeneous regions, though the heterogeneous PDE appears to decrease the variance. PINN-HH displays textural artifacts that reduce the resolution. PINN-het has fewer artifacts and better resolution of the smaller targets due to the lack of homogeneity assumption.

5.2 Incorporating Anatomical Information on Patient Data

For our next experiment, we obtained abdominal MRE from a study at the University of Pittsburgh Medical Center that included patients at least 18 years old who were diagnosed with non-alcoholic fatty liver disease (NAFLD) and underwent MRE between January 2016–2019 (demographic and image acquisition details can be found in Pollack et al. 2021 [22]). 155 patients had high-quality

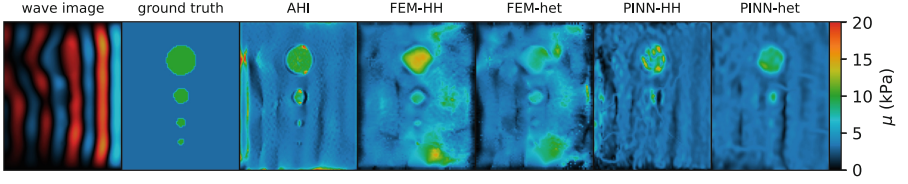


Fig. 4. Elasticity reconstruction examples on simulated data with no noise.

elastography, wave images, and anatomical MRI sequences. The wave images contained only one real displacement component and we did not have ground truth elasticity, so we used proprietary elastograms collected during the study as the “gold standard.” We registered MRI sequences (T1 pre in-phase, T1 pre water, T1 pre out-phase, T1 pre fat, and T2) to the MRE using SimpleITK v2.0.0 [30] and incorporated them as the anatomical features \mathbf{a} shown in Fig. 2. Liver regions were segmented using a previously reported deep learning model [22].

We performed elasticity reconstruction on each of the 155 patient wave images using each method. We investigated the influence of anatomical information when training PINNs by varying the anatomical loss weight λ_{anat} . Reconstruction fidelity was assessed using the Pearson correlation (R) between the predicted elasticity and the gold standard elasticity in the segmented liver regions.

Experiment Results. Figure 5A shows correlation distributions between predicted and gold standard elasticity across the different patients. PINN-het had the highest median correlation and least variation between patients (median = 0.84, IQR = 0.04). PINN-HH came in second (median = 0.76, IQR = 0.05) while FEM-het came in third, but had the most variability (median = 0.74, IQR = 0.19). FEM-HH performed slightly worse than FEM-het, but was less variable (median = 0.70, IQR = 0.11). AHI performed the worst on *in vivo* data (median = 0.63, IQR = 0.12) and had the greatest number of low outliers.

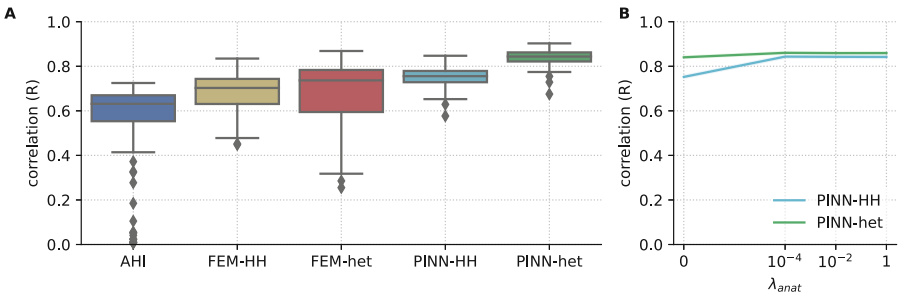


Fig. 5. Reconstruction performance on *in vivo* liver data. Figure 5A shows Pearson’s correlations between predicted and gold standard elasticity across patients. Figure 5B shows the effect of the anatomic loss weight on PINN elasticity reconstruction performance.

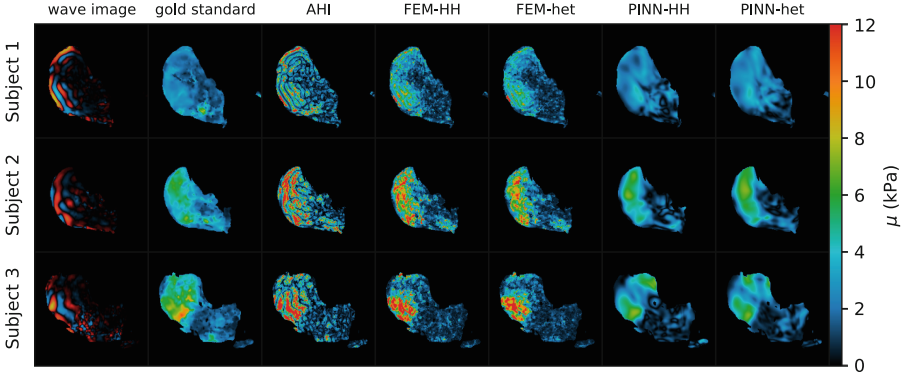


Fig. 6. Elasticity reconstruction examples for 3 patients from the NAFLD data set.

Figure 5B shows the effect of increasing the anatomic loss weight on PINN elasticity reconstruction quality. There was significant improvement in the correlation with the gold standard when the loss weight was increased from 0 to $1e-4$ for both PINN-HH ($p = 4.9e-56$) and PINN-het ($p = 3.0e-14$), but no significant difference from increasing it further to $1e-2$ for either method (PINN-HH: $p = 0.51$, PINN-het: $p = 0.23$). Raising the anatomic loss weight to $1e-4$ increased the median correlation from 0.76 to 0.85 in PINN-HH and from 0.84 to 0.87 in PINN-het. This suggests that there is a synergistic effect from including physical constraints and anatomical imaging data in elasticity reconstruction.

Figure 6 displays reconstructed elastograms for three randomly selected patients. AHI, FEM-HH and FEM-het all tend to overestimate the stiffness and have artifacts around nulls in the wave image. In contrast, PINN-HH and PINN-het more closely resemble the gold standard elastography, especially in regions close to the clinical threshold for fibrosis [31]. Furthermore, neither PINN reconstruction method shows signs of instabilities around wave amplitude nulls.

6 Conclusion

PINNs have several clinically significant advantages over conventional methods for tissue elasticity reconstruction in MRE. They are more robust to noise, which is pervasive in real MRE data. Furthermore, they can leverage anatomical information from other MRI sequences that are standard practice to collect during an MRE exam, and doing so significantly improves reconstruction fidelity. Limitations of this work include the use of the incompressibility assumption to simplify the training framework, and the relatively poor contrast on simulated data. This underscores how accurate reconstruction on simulated data does not always translate to real data, and vice versa. In future work, we will evaluate PINNs for solving the general form of the PDE to investigate the effect of the incompressibility assumption. We will also extend to an operator learning framework in which the model learns to solve the PDE in a generalizable fashion without the need to retrain on each wave image. This would reduce the computation cost and enable further integration of physics-informed and data-driven learning.

Acknowledgements & Data Use. This work was supported by the Pennsylvania Department of Health (grant number 41000873310), National Institutes of Health (grant number R01HL141813), the National Science Foundation (grant number 1839332) and Tripod+X. This work used the Bridges-2 system, which is supported by NSF award number OAC-1928147 at the Pittsburgh Supercomputing Center (PSC).

The patient MRE data was acquired by Amir A. Borhani, MD while he was at University of Pittsburgh. We thank him for his collaboration and guidance during this project.

References

1. Manduca, A., et al.: Magnetic resonance elastography: non-invasive mapping of tissue elasticity. *Med. Image Anal.* **5**(4), 237–254 (2001). [https://doi.org/10.1016/S1361-8415\(00\)00039-6](https://doi.org/10.1016/S1361-8415(00)00039-6)
2. Petitsclerc, L., Sebastiani, G., Gilbert, G., Cloutier, G., Tang, A.: Liver fibrosis: review of current imaging and MRI quantification techniques. *J. Magn. Reson. Imaging* **45**(5), 1276–1295 (2016)
3. Oliphant, T.E., Manduca, A., Ehman, R.L., Greenleaf, J.F.: Complex-valued stiffness reconstruction for magnetic resonance elastography by algebraic inversion of the differential equation. *Magn. Reson. Med.* **45**(2), 299–310 (2001). [https://doi.org/10.1002/1522-2594\(200102\)45:2<299::aid-mrm1039>3.0.co;2-o](https://doi.org/10.1002/1522-2594(200102)45:2<299::aid-mrm1039>3.0.co;2-o)
4. Park, E., Maniatty, A.M.: Shear modulus reconstruction in dynamic elastography: time harmonic case. *Phys. Med. Biol.* **51**, 3697 (2006). <https://doi.org/10.1088/0031-9155/51/15/007>
5. Papazoglou, S., Hamhaber, U., Braun, J., Sack, I.: Algebraic Helmholtz inversion in planar magnetic resonance elastography. *Phys. Med. Biol.* **53**(12), 3147–3158 (2008). <https://doi.org/10.1088/0031-9155/53/12/005>
6. Eskandari, H., Salcudean, S.E., Rohling, R., Bell, I.: Real-time solution of the finite element inverse problem of viscoelasticity. *Inverse Prob.* **27**(8), 085002 (2011). <https://doi.org/10.1088/0266-5611/27/8/085002>
7. Honarvar, M., Sahebjavaher, R., Sinkus, R., Rohling, R., Salcudean, S.E.: Curl-based finite element reconstruction of the shear modulus without assuming local homogeneity: Time harmonic case. *IEEE Tran. Med. Imaging* **32**(12), 2189–99 (2013). <https://doi.org/10.1109/TMI.2013.2276060>
8. Honarvar, M., Rohling, R., Salcudean, S.E.: A comparison of direct and iterative finite element inversion techniques in dynamic elastography. *Phys. Med. Biol.* **61**(8), 3026–48 (2016). <https://doi.org/10.1088/0031-9155/61/8/3026>
9. Fovargue, D., Nordsletten, D., Sinkus, R.: Stiffness reconstruction methods for MR elastography. *NMR Biomed.* **31**(10), e3935 (2018). <https://doi.org/10.1002/nbm.3935>
10. Fovargue, D., Kozerke, S., Sinkus, R., Nordsletten, D.: Robust MR elastography stiffness quantification using a localized divergence free finite element reconstruction. *Med. Image Anal.* **44**, 126–142 (2018)
11. Murphy, M.C., Manduca, A., Trzasko, J.D., Glaser, K.J., Huston III, J., Ehman, R.L.: Artificial neural networks for stiffness estimation in magnetic resonance elastography. *Magn. Reson. Med.* **80**(1), 351–360 (2017)
12. Solamen, L., Shi, Y., Amoh, J.: Dual objective approach using a convolutional neural network for magnetic resonance elastography. arXiv preprint: 1812.00441 [physics.med-ph] (2018)

13. Ni, B., Gao, H.: A deep learning approach to the inverse problem of modulus identification in elasticity. *MRS Bull.* **46**(1), 19–25 (2021). <https://doi.org/10.1557/s43577-020-00006-y>
14. Raissi, M., Perdikaris, P., Karniadakis, G.E.: Physics-informed neural networks: a deep learning framework for solving forward and inverse problems involving nonlinear partial differential equations. *J. Comput. Phys.* **378**, 686–707 (2019). <https://doi.org/10.1016/j.jcp.2018.10.045>
15. Haghighat, E., Raissi, M., Moure, A., Gomez, H., Juanes, R.: A physics-informed deep learning framework for inversion and surrogate modeling in solid mechanics. *Comput. Methods Appl. Mech. Eng.*, 113741 (2021). <https://doi.org/10.1016/j.cma.2021.113741>
16. Zhang, E., Yin, M., Karniadakis, G.E.: Physics-informed neural networks for nonhomogeneous material identification in elasticity imaging. arXiv preprint: 2009.04525 [cs.LG] (2020). <https://doi.org/10.48550/arXiv.2009.04525>
17. Mallampati, A., Almekkawy, M.: Measuring tissue elastic properties using physics based neural networks. In: 2021 IEEE UFFC Latin America Ultrasonics Symposium (LAUS), pp. 1–4. IEEE, Gainesville (2021). <https://doi.org/10.1109/LAUS53676.2021.9639231>
18. Kamali, A., Sarabian, M., Laksari, K.: Elasticity imaging using physics-informed neural networks: spatial discovery of elastic modulus and Poisson’s ratio. *Acta Biomater.* **155**, 400–409 (2023). <https://doi.org/10.1016/j.actbio.2022.11.024>
19. Wymer, D.T., Patel, K.P., Burke, W.F., III., Bhatia, V.K.: Phase-contrast MRI: physics, techniques, and clinical applications. *RadioGraphics* **40**(1), 122–140 (2020)
20. Sinkus, R., Daire, J.L., Beers, B.E.V., Vilgrain, V.: Elasticity reconstruction: beyond the assumption of local homogeneity. *Comptes Rendus Mécanique* **338**(7), 474–479 (2010). <https://doi.org/10.1016/j.crme.2010.07.014>
21. Honarvar, M.: Dynamic elastography with finite element-based inversion. Ph.D. thesis, University of British Columbia (2015). <https://doi.org/10.14288/1.0167683>
22. Pollack, B.L., et al.: Deep learning prediction of voxel-level liver stiffness in patients with nonalcoholic fatty liver disease. *Radiology: AI* **3**(6) (2021). <https://doi.org/10.1148/ryai.2021200274>
23. Sitzmann, V., Martel, J.N.P., Bergman, A.W., Lindell, D.B., Wetzstein, G.: Implicit neural representations with periodic activation functions (2020)
24. Kingma, D.P., Ba, J.L.: Adam: a method for stochastic optimization. In: *Proceedings of 3rd International Conference Learning Representations* (2015)
25. Paszke, A., et al.: PyTorch: an imperative style, high-performance deep learning library. In: *Advance Neural Information Processing System*, vol. 32, pp. 8024–8035. Curran Associates, Inc. (2019)
26. Lu, L., Meng, X., Mao, Z., Karniadakis, G.E.: DeepXDE: a deep learning library for solving differential equations. *SIAM Rev.* **63**(1), 208–228 (2021). <https://doi.org/10.1137/19M1274067>
27. Scroggs, M.W., Dokken, J.S., Richardson, C.N., Wells, G.N.: Construction of arbitrary order finite element degree-of-freedom maps on polygonal and polyhedral cell meshes. *ACM Trans. Math. Softw.* **48**, 1–23 (2022). <https://doi.org/10.1145/3524456>
28. Barnhill, E., Davies, P.J., Ariyurek, C., Fehlner, A., Braun, J., Sack, I.: Heterogeneous multifrequency direct inversion (HMDI) for magnetic resonance elastography with application to a clinical brain exam. *Med. Image Anal.* **46**, 180–188 (2018). <https://doi.org/10.1016/j.media.2018.03.003>

29. Kallel, F., Bertrand, M., Ophir, J.: Fundamental limitations on the contrast-transfer efficiency in elastography: an analytic study. *Ultrasound Med. Biol.* **22**(4), 463–470 (1996). [https://doi.org/10.1016/0301-5629\(95\)02079-9](https://doi.org/10.1016/0301-5629(95)02079-9)
30. Lowekamp, B.C., Chen, D.T., Ibáñez, L., Blezek, D.: The design of SimpleITK. *Front. Neuroinf.* **7**(45) (2013). <https://doi.org/10.3389/fninf.2013.00045>
31. Mueller, S., Sandrin, L.: Liver stiffness: a novel parameter for the diagnosis of liver disease. *Hepat. Med.* **2**, 49–67 (2010). <https://doi.org/10.2147/hmer.s7394>